ACS APPLIED MATERIALS & INTERFACES

www.acsami.org

Research Article

Long-Range Proton Transport in Films from a Reflectin-Derived Polypeptide

Chengyi Xu, Nabin Kandel, Xin Qiao, Md. Imran Khan, Preeta Pratakshya, Nadia E. Tolouei, Bo Chen,* and Alon A. Gorodetsky*

Cite This: https://doi.org/10.1021/acsami.0c18929

Read Online

ACCESS | Metrics & More | Article Recommendations | Supporting Information

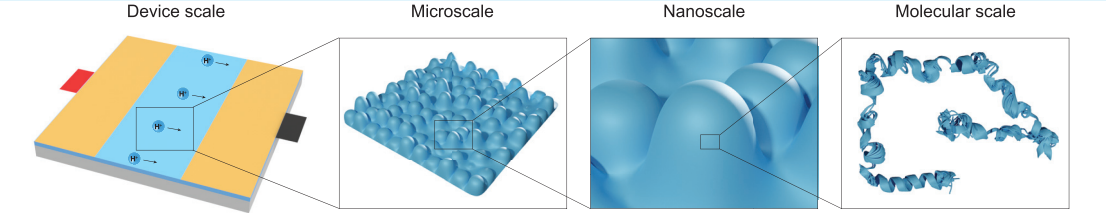

ABSTRACT: Protein- and peptide-based proton conductors have been extensively studied because of their important roles in biological processes and established potential for bioelectronic device applications. However, despite much progress, the demonstration of long-range proton transport for such materials has remained relatively rare. Herein, we fabricate, electrically interrogate, and physically characterize films from a reflectin-derived polypeptide. The electrical measurements indicate that device-integrated films exhibit proton conductivities with values of ∼0.4 mS/cm and sustain proton transport over distances of ∼1 mm. The accompanying physical characterization indicates that the polypeptide possesses characteristics analogous to those of the parent protein class and furnishes insight into the relationship between the polypeptide's electrical functionality and structure in the solid state. When considered together, our findings hold significance for the continued development and engineering of not only reflectin-based materials but also other bioinspired proton conductors.

KEYWORDS: *reflectin, proteins, proton conduction, self-assembly, solid-state NMR*

INTRODUCTION

Natural materials that support proton transport have been extensively studied because of their important roles in biological processes and established potential for applications in bioelectronic devices.[1−10] In particular, protein- and peptide-based proton conductors have been touted as especially promising because of their numerous desirable characteristics, which include modular sequences, controllable self-assembly properties, programmable functionalities, and good biocompatibilities.[6−10] However, despite much progress, naturally derived or designer proteinaceous conductors that effectively transport protons over long distances of ∼0.01 mm to ∼10 mm remain comparatively rare, with few examples reported to date.[11−16] For instance, Silberbush and co-workers have explored the proton conductivity of self-assembled films from amyloid β peptides over a distance of ∼0.02 mm.[14] In addition, Amdursky and co-workers have studied proton transfer in electrospun mats from bovine serum albumin over a distance of ∼2.5 mm.[15] Furthermore, Pena-Francesch and co-workers have investigated proton transport in dropcast films from squid ring teeth proteins over a distance of ∼7 mm.[16] Accordingly, given such exciting combined precedent, there has emerged an opportunity for the continued development of protein- and peptide-based systems that support long-range proton conduction.

Within the context of protein-based proton conductors, our laboratory has focused on exploring the electrical properties of cephalopod structural proteins known as reflectins.[10,17−23] These proteins were initially definitively isolated from the reflective platelets of the *Euprymna scolopes* (*E. scolopes*) squid (Figure 1A), and their amino acid sequences were immediately benchmarked as unusual due to the prevalence of specific conserved repeating motifs and high aromatic, charged, and polar residue contents (Figure 1B).[24] The isolated *E. scolopes* reflectin isoforms (and their variants) were subsequently found to exhibit exquisite sensitivity to changes in environmental conditions and to spontaneously self-assemble into nanoparticles (Figure 1C).[25,26] Various reflectins were also shown to be compatible with multiple thin-film processing methods, e.g., drop-casting, spin-casting, dip-coating, and inkjet printing,

Received: October 21, 2020
Accepted: March 2, 2021

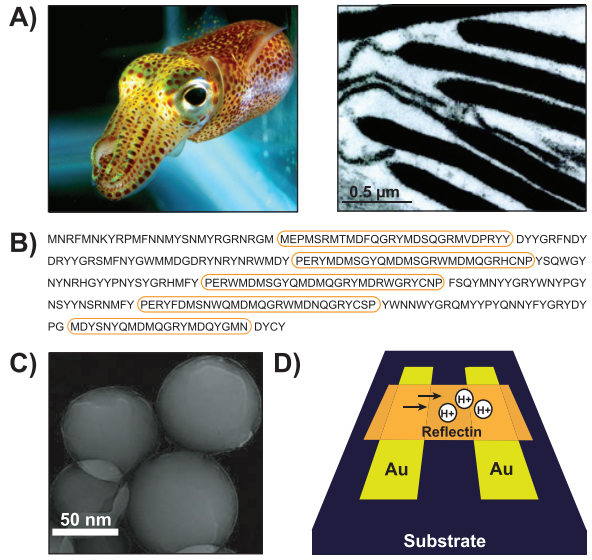

Figure 1. (A) Picture of an *E. scolopes* squid (left) and a transmission electron microscopy (TEM) image of its reflectin-based platelets (right).[24] (B) Amino acid sequence of *E. scolopes* reflectin 1b, where the general forms of the conserved domains are indicated with orange ovals.[24] (C) TEM image of spheroidal nanoparticles self-assembled from *E. scolopes* reflectin 1a.[25] (D) Schematic of a representative two-terminal proton-conducting device from *D. pealeii* reflectin variants.

and could even withstand relatively harsh fabrication protocols, e.g., direct metal depositions.[17−23,25−30] When incorporated into two-terminal devices, the reflectin-based films fabricated via drop-casting revealed room-temperature proton conductivities of ∼0.07 mS/cm to ∼0.1 mS/cm over distances of ∼0.05 mm to ∼0.1 mm for *D. pealeii* reflectins A1 and A2 (Figure 1D).[18,19] Such electrical properties enabled the development of more advanced reflectin-based bioelectronic platforms, including protonic transistors,[18,20] photochemically dopable systems,[21] and protochromic devices.[22] However, despite much progress, the electrical properties of reflectins from species other than *D. pealeii* were not reported, long-range proton conduction over millimeter length scales in reflectin films was not investigated, and the relationship between the molecular structure and electrical function of reflectin-based materials was not completely elucidated.

Herein, we investigate the electrical properties and structural characteristics of films fabricated from a reflectin-derived polypeptide. First, we select a known recombinant reflectin variant and characterize its solution-phase assembly via dynamic light scattering (DLS) measurements, ultraviolet−visible (UV/Vis) spectroscopy, and circular dichroism (CD) spectroscopy. Second, we prepare two-terminal devices from reflectin-derived polypeptide films via standard fabrication methods and electrically interrogate them with electrochemical impedance spectroscopy (EIS) under different environmental conditions. Third, we explore our films' morphologies with atomic force microscopy (AFM) and scanning electron microscopy (SEM) and their global structural ordering with Fourier transform infrared (FTIR) spectroscopy and solid-state CD spectroscopy. Last, we probe the local molecular-level order of the reflectin-derived polypeptides comprising our films via solid-state nuclear magnetic resonance (ssNMR) spectroscopy. Altogether, our work holds relevance for understanding and engineering not only reflectin-based materials specifically but also other protein-based proton conductors more generally.

SELECTION AND SOLUTION-PHASE CHARACTERIZATION OF A REFLECTIN-DERIVED POLYPEPTIDE

We began our efforts by selecting a recombinant reflectin-derived polypeptide previously designed and studied by Dennis and co-workers.[27] The primary sequence of the polypeptide, which was denoted as Ref(2C)$_4$ in accordance with literature precedent, is illustrated in Figure 2A.[27] The sequence incorporated four repeats of the amino acid tract DPRYY-DYYGRFNDYDRYYGRSMF from *E. scolopes* reflectin 1b, contained intervening linker regions between these repeats, and featured an N-terminal histidine tag (Figure 2A).[27] In analogy to the parent native protein, Ref(2C)$_4$ contained a high proportion of aromatic (e.g., Tyr and Phe), charged (e.g., Asp and Arg), and uncharged polar (e.g., Ser and Thr) residues (Figure 2A).[27] Consequently, Ref(2C)$_4$ recapitulated some of the related reflectins' key characteristics, such as processability into thin films, environmental stability, and stimuli-responsive light scattering functionality.[26,27] Moreover, this designer polypeptide was relatively more tractable and amenable to purification in the quantities desirable for material experiments.[26,27] Given the above considerations, Ref(2C)$_4$ con-

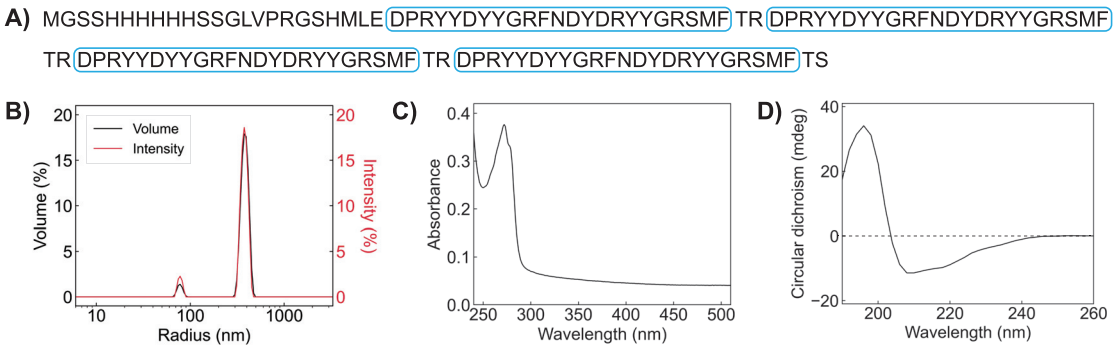

Figure 2. (A) Amino acid sequence of Ref(2C)$_4$, which incorporates four identical amino acid tracts (blue ovals). (B) Representative DLS volume (black) and intensity (red) distributions obtained for solutions of Ref(2C)$_4$. (C) Representative UV/Vis absorbance spectrum obtained for solutions of Ref(2C)$_4$. (D) Representative CD spectrum obtained for solutions of Ref(2C)$_4$.

https://doi.org/10.1021/acsami.0c18929
ACS Appl. Mater. Interfaces XXXX, XXX, XXX−XXX

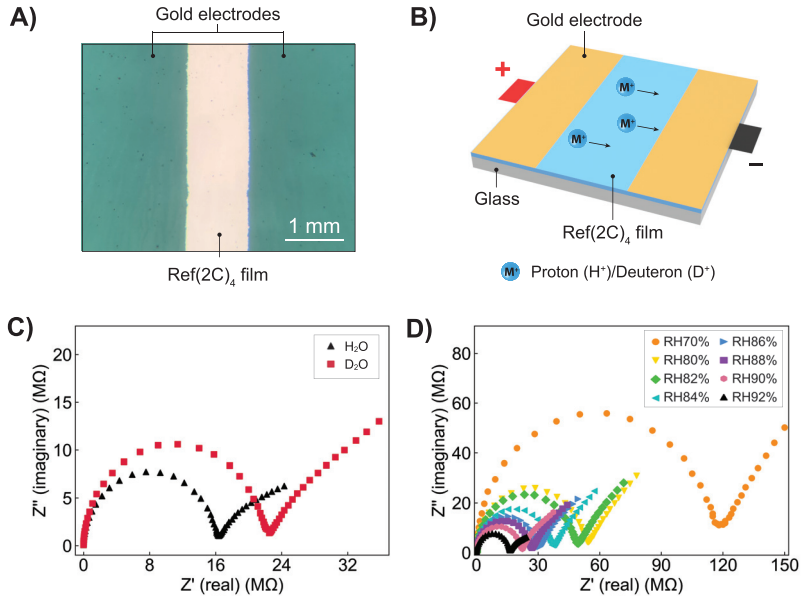

Figure 3. (A) Representative optical microscopy image of part of a two-terminal device, wherein a Ref(2C)$_4$ film is contacted by two gold electrodes with a separation of ∼1 mm. (B) Schematic of the long-range transport of protons and deuterons for a device-integrated Ref(2C)$_4$ film. (C) Nyquist plots obtained for a representative two-terminal device from a Ref(2C)$_4$ film in the presence of H_2O (black triangles) and D_2O (red squares) vapor at a relative humidity of 92%. (D) Nyquist plots obtained for the same representative two-terminal device in the presence of H_2O vapor at relative humidities of 70% (orange), 80% (yellow), 82% (green), 84% (turquoise), 86% (blue), 88% (purple), 90% (pink), and 92% (black). Note that the same Nyquist plots are shown in (C) and (D) for H_2O vapor at a relative humidity of 92% in order to facilitate direct comparisons.

stituted a judicious target biomolecule for electrical measurements and structural characterization.

We in turn investigated the properties of the recombinant reflectin-derived polypeptide in solution. Toward this end, we initially expressed, purified, and isolated Ref(2C)$_4$ according to entrenched literature procedures.[25−27] We then solubilized this polypeptide in hexafluoro-2-propanol (HFIP), an organic solvent well known to stabilize protein secondary structures and promote the formation of helices.[31,32] We subsequently probed such solutions with DLS measurements, UV/Vis spectroscopy, and CD spectroscopy (Figure 2B−D). The DLS volume and intensity size distributions revealed the presence of two distinct populations with hydrodynamic radii of ∼80 nm and ∼350 nm, indicating that the polypeptide primarily formed nanoparticles (Figure 2B). The UV/Vis absorption spectrum revealed a peak at ∼272 nm and tailing at higher wavelengths, which was consistent with a high aromatic amino acid content and the presence of scattering nanostructures (Figure 2C).[33,34] The CD spectrum revealed a positive peak at ∼196 nm and two negative peaks at ∼208 nm and ∼220 nm, suggesting that the polypeptide contained α-helices but also featured some β-character in solution (Figure 2D).[35,36] Notably, the observations were consistent with reports not only for full length *E. scolopes* reflectins but also for their recombinant variants under analogous conditions.[25−27] When considered together, our measurements provided insight into Ref(2C)$_4$'s aggregation state and secondary structural characteristics.

FABRICATION AND ELECTRICAL INTERROGATION OF REFLECTIN-DERIVED POLYPEPTIDE FILMS

Having selected the reflectin-derived polypeptide and characterized its assembly states in solution, we proceeded to prepare two-terminal devices from the material. For this purpose, we adopted the methodologies previously validated for various reflectin-based platforms.[17−23,25−30] The corresponding general fabrication scheme is illustrated in Figure S1. In brief, we first spin-cast our Ref(2C)$_4$ nanoparticle solutions (with HFIP as the solvent) onto glass substrates, forming films with areas of several square centimeters (Figure S1). We next stored the just-cast films in ambient atmosphere, enabling evaporation of any residual HFIP (Figure S1). We in turn electron-beam-evaporated two gold electrodes with a separation (gap) of ∼1 mm directly onto the dried films, completing the desired devices (Figure S1). As an illustrative example, an optical microscopy image of the active area of one resulting device is shown in Figure 3A. This robust and straightforward fabrication strategy facilitated the throughput of the ensuing electrical measurements.

We next electrically interrogated the two-terminal devices from the reflectin-derived polypeptide films under different environmental conditions. For this purpose, we specifically used electrochemical impedance spectroscopy (EIS) in order to facilitate interpretation of our measurements and afford comparisons with other protein- and peptide-based proton conductors.[11−13,15,16,18,19,23] A schematic depicting the transport of charge carriers (i.e., protons or deuterons) in our device-integrated Ref(2C)$_4$ films is shown in Figure 3B, and representative Nyquist plots obtained for such devices in the presence of water (H_2O) or deuterium oxide (D_2O) vapor at a relative humidity (RH) of 92% are shown in Figure 3C. In general, the Nyquist plots revealed semicircles in the high-frequency region, which were attributed to the bulk impedance of a conductive film, and inclined spurs with concave curvature in the low frequency region, which were attributed to the interfacial impedance of a non-ideal, i.e., potentially rough, film/electrode contact (Figure 3C).[18,37,38] These experimental measurements were readily modeled with an equivalent circuit

https://doi.org/10.1021/acsami.0c18929
ACS Appl. Mater. Interfaces XXXX, XXX, XXX−XXX

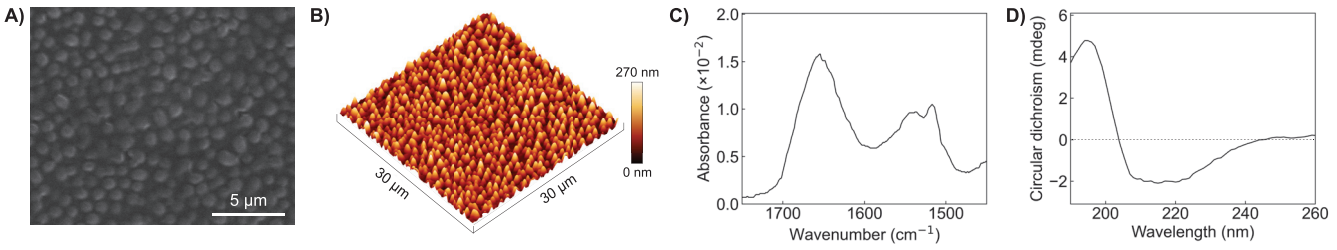

Figure 4. (A) Representative SEM image obtained for a Ref(2C)$_4$ film. (B) Representative AFM topographic image obtained for a Ref(2C)$_4$ film. (C) Representative FTIR absorbance spectrum obtained for a Ref(2C)$_4$ film. (D) Representative solid-state CD spectrum obtained for a Ref(2C)$_4$ film.

in which the bulk impedance was represented by an RC loop containing a bulk resistance element (R_{bulk}) and a bulk capacitance element (C_{bulk}) and the interfacial impedance was represented by an RC loop containing an interfacial resistance element (R_{int}) and an interfacial constant phase element (CPE_{int}) (Figure S2, Figure S3, and Table S1).[18,37,38] The experiments and modeling indicated that our films featured an average conductivity of 0.41 ± 0.06 mS/cm in the presence of H_2O, presumably corresponding to bulk proton transport, and an average conductivity of 0.29 ± 0.06 mS/cm in the presence of D_2O, presumably corresponding to bulk deuteron transport (note also the different diameters of the semicircles in the high-frequency region) (Figure 3B,C, Figure S3, and Table S1). Upon moving from H_2O to D_2O *in situ*, the 29 ± 5% decrease in the conductivity was consistent with predictions and measurements of the kinetic isotope effect for protein-based proton conductors (Figure 3B,C).[11−13,15,16,18,19,23,39] Notably, the proton conductivities found for Ref(2C)$_4$ films were ∼4-fold to ∼8-fold greater than those previously reported for inkjet printed and dropcast *D. pealeii* reflectin A1 films under similar conditions.[18,23] Overall, the measurements suggested that Ref(2C)$_4$ was a highly effective proton-conducting material.

We further electrically probed the two-terminal devices from the reflectin-derived polypeptide films as a function of systematic changes in the environmental conditions. For this purpose, we again leveraged EIS to facilitate straightforward interpretation and benchmarking of our measurements.[11−13,15,16,18,19,23,40] The representative Nyquist plots obtained for our devices in the presence of H_2O vapor at RH values between 70% and 92% are shown in Figure 3D. The Nyquist plots revealed semicircles consistent with the bulk impedances of conductive films and inclined concave spurs consistent with the interfacial impedances of non-ideal film/electrode contacts (Figure 3D).[18,37,38] These experimental measurements could again be faithfully modeled with our equivalent circuit, reinforcing the likely accuracy of the physical interpretation (Figure S2, Figure S4, and Table S2). The model indicated that the conductivity of our representative film systematically decreased from a value of ∼0.31 mS/cm at an RH of 92% to a value of ∼0.04 mS/cm at an RH of 70% (Figure 3D, Figure S4, and Table S2). Moreover, our films' calculated conductivity featured a logarithmic dependence on the relative humidity, which was consistent with expectations for proton-conducting materials (Figure S5).[40,41] Excitingly, the device-integrated Ref(2C)$_4$ films transported protons over a distance of ∼1 mm at different relative humidities, which was ∼10-fold to ∼20-fold greater than the distances previously reported for device-integrated *D. pealeii* reflectin A1 and reflectin A2 films at comparable RH values.[18,19,23] Taken together, these measurements further underscored Ref(2C)$_4$'s excellent proton-conducting functionality.

MORPHOLOGICAL AND STRUCTURAL CHARACTERIZATION OF REFLECTIN-DERIVED POLYPEPTIDE FILMS

To better understand the electrical functionality of the reflectin-derived polypeptide films, we characterized their microscale and nanoscale morphologies. For this purpose, we imaged our films with SEM and AFM, enabling direct comparisons with assembled architectures from other *E. scolopes* reflectin variants.[25−27] The SEM and AFM images obtained for the Ref(2C)$_4$ films are shown in Figure 4A,B. The SEM images revealed that the films' surfaces consisted of randomly distributed and densely packed spheroidal domains with estimated radii between ∼50 nm and ∼400 nm (Figure 4A). The three-dimensional topographic AFM images analogously showed that the films' surfaces consisted of protruding comparably sized spheroidal domains and featured substantial average root-mean-square (RMS) surface roughnesses of ≳40 nm (Figure 4B). Here, the constituent domains' estimated sizes in the solid state were in reasonable agreement with those found for Ref(2C)$_4$ nanoparticles in solution (Figure 2B), especially when accounting for crowding- and substrate-induced geometric distortions.[30] In addition, the nanostructured topographies generally resembled those reported for other *E. scolopes* recombinant reflectins in the solid state.[26,27] Notably, the significant roughness of our films provided a physical explanation for the presence of non-ideal (presumably rough) film/electrode interfaces in our two-terminal devices, as indicated by our equivalent circuit model (see Figure S2 and *vide supra*). Consequently, the microscopy measurements revealed the Ref(2C)$_4$ films' micro- to nanoscale organization and afforded added insight into the electrical performance of our devices.

We subsequently assessed the presence of global structural order, i.e., specific secondary structure, within the reflectin-derived polypeptide films. For this purpose, we used a combination of FTIR spectroscopy and CD spectroscopy, enabling comparisons with the secondary structural characteristics reported for other *E. scolopes* reflectins.[25−27] The FTIR and solid-state CD spectra obtained for our Ref(2C)$_4$ films are shown in Figure 4C,D. The FTIR spectra revealed a peak with a maximum at ∼1654 cm^{-1} (in the Amide I band) and a peak with two maxima at ∼1536 cm^{-1} and ∼1520 cm^{-1} (in the Amide II band), thus indicating that Ref(2C)$_4$ possessed primarily an α-helical secondary structure and also some β-character in the solid state (Figure 4C).[42,43] The solid-state CD spectrum revealed a positive peak at ∼194 nm and a

https://doi.org/10.1021/acsami.0c18929
ACS Appl. Mater. Interfaces XXXX, XXX, XXX−XXX

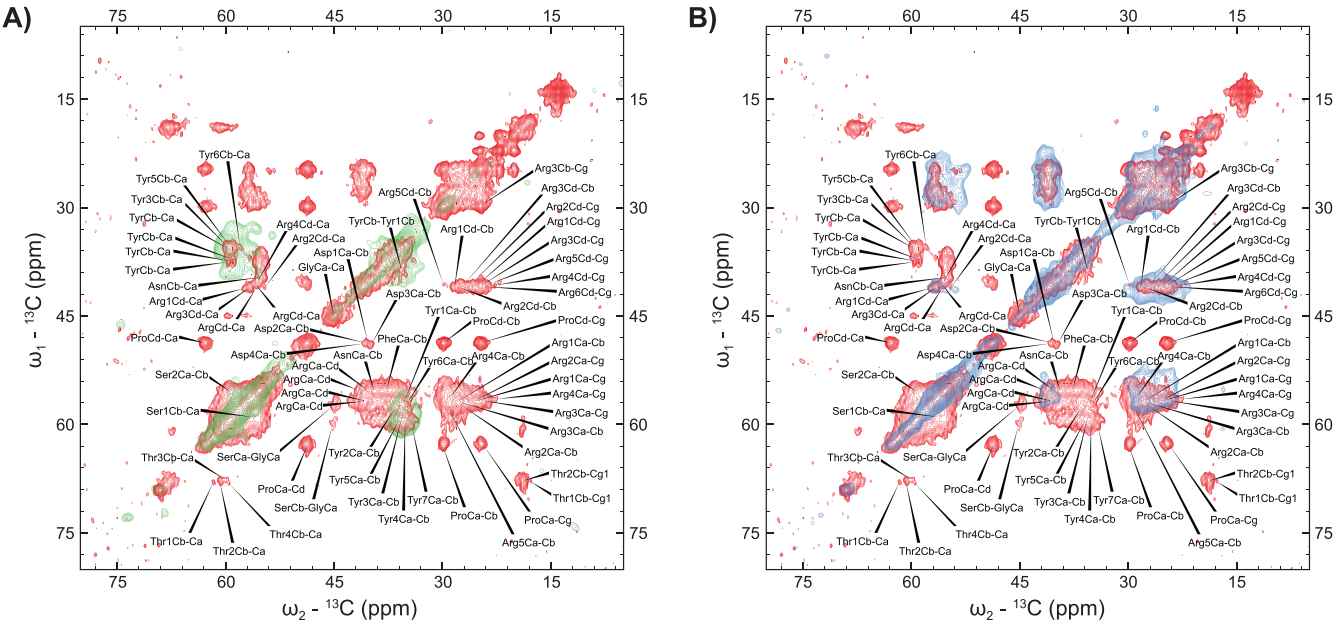

Figure 5. (A) Representative 2D $^{13}C-^{13}C$ correlation ssNMR spectra obtained for uniformly ^{13}C- and ^{15}N-labeled Ref(2C)$_4$ (red contours) and selectively Tyr-labeled Ref(2C)$_4$ (green contours). (B) Representative 2D $^{13}C-^{13}C$ correlation ssNMR spectra obtained for uniformly ^{13}C- and ^{15}N-labeled Ref(2C)$_4$ (red contours) and selectively Arg-labeled Ref(2C)$_4$ (blue contours). Note that identical spectra are shown in (A) and (B) for uniformly ^{13}C- and ^{15}N-labeled Ref(2C)$_4$ (red contours) in order to facilitate direct comparisons.

negative broad peak between ∼204 nm and ∼240 nm, again indicating that Ref(2C)$_4$ contained both α-helices and β-sheets in the solid state (Figure 4D).[35,36] Notably, the secondary structure of Ref(2C)$_4$ in films was not only comparable to that found for Ref(2C)$_4$ nanoparticles in solution (Figure 2D) but also matched prior observations of secondary structural characteristics for full-length reflectin 1a and truncated recombinant reflectin 1a.[25,26] The spectroscopic measurements thus suggested that the assembly state of Ref(2C)$_4$ in nanoparticles was generally maintained during the formation of nanostructured proton-conducting films.

MOLECULAR-LEVEL CHARACTERIZATION OF REFLECTIN-DERIVED POLYPEPTIDE FILMS

After gaining insight into our films' global morphologies and structural order, we developed a strategy for better understanding the molecular-level conformations and secondary structures of the reflectin-derived polypeptides in the solid state. For this purpose, we expressed, purified, and isolated uniformly ^{13}C- and ^{15}N-labeled, selectively Tyr-labeled, and selectively Arg-labeled Ref(2C)$_4$ according to literature procedures.[25−27,44] We then processed the labeled peptides into films analogous to those used both for electrical measurements and for global morphological and structural characterization, i.e., casting followed by solvent evaporation. We next transferred the various films to NMR rotors and recorded the 2D $^{13}C-^{13}C$ correlation ssNMR spectra. In such spectra, the positions of the different amino acids' resonances relative to the positions tabulated for the same amino acids in random coils (i.e., the ^{13}C signal upshifts and downshifts) furnish insight into the likely associated secondary structures, and the presence of cross-peaks for different amino acids (due to polarization transfer between sites) furnishes insight into the likely inter- or intra-residue contacts and/or proximities.[45−48] Moreover, the linewidths of the resonances in the spectra provide additional information on both the residues' secondary structural characteristics and local molecular motion/flexibility.[47−50] Accordingly, we postulated that a detailed analysis of the obtained spectra would yield a nuanced understanding of self-assembled Ref(2C)$_4$'s molecular-level order in the solid state.

We initially identified and assigned the signals corresponding to our reflectin-derived polypeptides' Gly, Pro, Thr, and Ser residues. For this purpose, we examined the aliphatic regions of the 2D $^{13}C-^{13}C$ correlation spectra collected for films from uniformly ^{13}C- and ^{15}N-labeled Ref(2C)$_4$. The Gly residues exhibited a single set of resonances centered at C_a ∼45.0 ppm, for which the C_a upshifts indicated an α-helical character (Figure 5A,B (red contours) and Table S3). The Gly residues' signals featured relatively narrow linewidths of ∼1.2 to ∼2 ppm, suggesting ordered backbone conformations (Figure 5A,B (red contours) and Table S3). The Pro residues exhibited two sets of resonances centered at C_a ∼62.9 ppm and C_b ∼29.9 ppm, for which the C_a upshifts and C_b downshifts again indicated a likely helical character (Figure 5A,B (red contours) and Table S3). The Pro residues' signals featured quite narrow linewidths of ∼1 ppm, again suggesting an ordered backbone conformation (Figure 5A,B (red contours) and Table S3). The Thr residues displayed multiple sets of resonances with a particularly dominant signal centered at C_a ∼60.7 ppm and C_b ∼67.8 ppm, for which the C_a upshifts and C_b downshifts again indicated an α-helical character (Figure 5A,B (red contours) and Table S3). The Thr residues' multiple signals featured relatively narrow linewidths of ∼1.2 to ∼2 ppm, suggesting partially ordered but distinguishable backbone conformations (Figure 5A,B (red contours) and Table S3). The Ser residues displayed multiple sets of strong resonances with signals centered at C_a ∼55.4 ppm and C_b ∼59.4 ppm as well as at C_a ∼55.7 ppm and C_b ∼59.1 ppm, for which the C_b downshifts were consistent with multiple different helix arrangements (Figure 5A,B (red contours) and Table S3). The Ser residues' signals all featured comparatively broad linewidths of >2 ppm,

https://doi.org/10.1021/acsami.0c18929
ACS Appl. Mater. Interfaces XXXX, XXX, XXX−XXX

suggesting disordered backbone conformations (Figure 5A,B (red contours) and Table S3). Notably, the consistent observation of α-helical character was in agreement with the interpretation of the FTIR and CD spectroscopy measurements performed for the films (Figure 4C,D). The detailed analysis revealed that some of Ref(2C)$_4$'s aliphatic amino acids (i.e., Gly and Pro) and polar uncharged amino acids (i.e., Thr) were locally ordered (i.e., associated with α-helical structures).

We next identified and assigned the signals corresponding to our reflectin-derived polypeptides' Asp and Asn residues. For this purpose, we examined the aliphatic and carbonyl regions of the 2D ^{13}C−^{13}C correlation spectra collected for films from uniformly ^{13}C- and ^{15}N-labeled Ref(2C)$_4$. The Asp residues displayed multiple closely spaced resonances centered at C_a ∼48.8 ppm and C_b ∼40.3 ppm within the aliphatic region, for which the C_a downshifts indicated a likely β-type character (Figure 5A,B (red contours) and Table S3), and these residues also displayed characteristic C_g resonances between ∼177.7 ppm and ∼179.5 ppm within the carbonyl region, which were typical of aspartic acid and corroborated the initial assignment (Figures S6 (red contours) and Figure S7 (red contours)). The Asp residues' pronounced C_a and C_b signals featured relatively narrow linewidths of ∼1.3 ppm, which were consistent with conformational order, as well as reduced intensities compared to the signals of amino acids less prevalent in Ref(2C)$_4$'s primary sequence, e.g., Pro, suggesting high side chain motion/flexibility (Figure S8 and Table S3). The Asn residues displayed resonances centered at C_a ∼55.3 ppm and C_b ∼40.3 ppm within a congested area of the aliphatic region, for which the C_a upshifts indicated some α-helical character (Figure 5A,B (red contours) and Table S3), and these residues also displayed strong overlapping C_g resonances at ∼176.8 ppm within the carbonyl region, which were typical of asparagine and corroborated the initial assignment (Figure S6 (red contours) and Figure S7 (red contours)). The Asn residues' C_g signals featured relatively narrow linewidths of ∼1.5 ppm, which were again consistent with conformational order (Figure S6 (red contours), Figure S7 (red contours), and Table S3). Notably, the observation of both β-type character and α-helical character further reinforced the interpretation of the FTIR and CD spectroscopy measurements performed for our films (Figure 4C,D). The detailed analysis revealed that Ref(2C)$_4$'s negatively charged amino acids (i.e., Asp) were not only locally ordered (i.e., associated with β-type structures) but likely mobile and that some of Ref(2C)$_4$'s polar uncharged amino acids (i.e., Asn) were also locally ordered (i.e., associated with α-helical structures).

We in turn identified and assigned the signals corresponding to our reflectin-derived polypeptides' Tyr and Phe residues. For this purpose, we examined the aliphatic and aromatic regions of the 2D ^{13}C−^{13}C correlation spectra collected for films from uniformly ^{13}C- and ^{15}N-labeled and selectively Tyr-labeled Ref(2C)$_4$. The Tyr residues exhibited multiple sets of overlapping resonances at C_a ∼57.2 to ∼57.7 ppm and C_b ∼35.2 to ∼35.6 ppm within the aliphatic region, for which the C_a upshifts and C_b downshifts both indicated an α-helical character (Figure 5A (red and green contours) and Table S3), and these residues also exhibited characteristic overlapped C_z resonances at ∼155.3 to ∼156.1 ppm within the aromatic regions of both ^{13}C- and ^{15}N-labeled and selectively Tyr-labeled Ref(2C)$_4$ (Figure S6, red and green contours). The various Tyr residues' C_a and C_b signals featured relatively narrow linewidths of ∼1.5 ppm, which suggested the presence of ordered arrangements, and their distinctive C_b cross-peaks intimated that some of the tyrosines were in close proximity to one another and likely interacting via pi−pi stacking (Figure 5A (red and green contours) and Table S3). The Phe residues displayed a dense resonance cluster centered at C_a ∼55.3 ppm and C_b ∼37.9 ppm, for which the C_b downshifts indicated an α-helical character (Figure 5A (red contours) and Table S3). The various Phe residues' clustered C_a and C_b signals featured broad linewidths of ∼3 ppm, which suggested the likely presence of significant local disorder (Figure 5A (red contours) and Table S3). The overall analysis showed that Ref(2C)$_4$'s aromatic amino acids adopted either ordered and presumably stacked arrangements (i.e., Tyr) or comparatively disordered arrangements (i.e., Phe).

We subsequently identified and assigned the signals corresponding to our reflectin-derived polypeptides' Arg residues. For this purpose, we examined the aliphatic and imine regions of the 2D ^{13}C−^{13}C correlation spectra collected for films from uniformly ^{13}C- and ^{15}N-labeled and selectively Arg-labeled Ref(2C)$_4$. The Arg residues displayed multiple sets of overlapping resonances between C_a ∼53.6 ppm to ∼56.7 ppm and C_b ∼27.4 ppm to ∼28.2 ppm within the aliphatic region, for which the C_a upshifts and C_b downshifts indicated an α-helical character (Figure 5B (red and blue contours) and Table S3). The Arg residues also displayed multiple sets of overlapping resonances between ∼23.9 ppm to ∼25.8 ppm and ∼41.0 ppm to ∼42.3 ppm in the aliphatic region and between ∼156.3 ppm to ∼157.4 ppm in the imine region for both ^{13}C- and ^{15}N-labeled and selectively Arg-labeled Ref(2C)$_4$ (Figure 5B (red and blue contours), Figure S7 (red and blue contours), and Table S3). The different Arg residues' numerous signals featured typically narrow linewidths of <2 ppm, suggesting multiple distinct but presumably ordered backbone conformations (Figure 5B (red and blue contours), Figure S7 (red and blue contours), and Table S3). Here, a subset of the signals observed for the uniformly and selectively labeled polypeptides did feature imperfect agreement, presumably due to slight differences in the film fabrication conditions. The overall analysis showed that Ref(2C)$_4$'s positively charged amino acids (i.e., Arg) formed a heterogeneous distribution of ordered arrangements.

We last studied how our ssNMR spectra were affected by subtle changes in the film preparation conditions. This effort was motivated by the well-known sensitivity of reflectins to their surrounding environment and to variation of processing parameters.[17−23,25−30] Thus, we performed ssNMR experiments for multiple films that were fabricated via casting of a Ref(2C)$_4$ solution onto a substrate and then directly transferred to a rotor. The spectra obtained for these films resembled one another in most respects when accounting for expected inherent experimental variability (compare, for example, the spectra in Figure 5 and Figure S9). Moreover, we performed ssNMR experiments for films that were prepared via repetitive casting of a Ref(2C)$_4$ solution into a rotor and evaporation of the solvent. The spectra obtained for such films displayed some differences in their specific signals but generally furnished similar molecular-level structural information (compare, for example, the spectra in Figures S9 and S10). Together, these observations underscored the reliability of our general film fabrication approach and portended favorably for the continued exploration of Ref(2C)$_4$'s self-assembly and structure in the solid state.

https://doi.org/10.1021/acsami.0c18929
ACS Appl. Mater. Interfaces XXXX, XXX, XXX−XXX

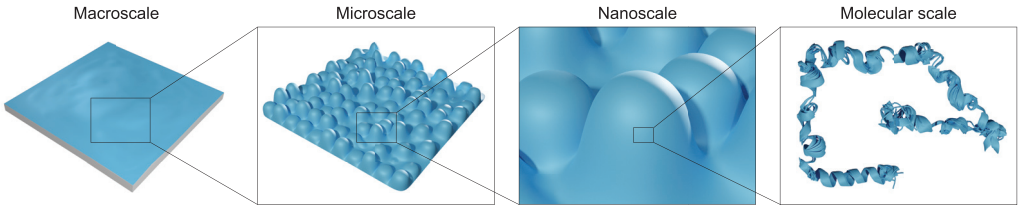

Figure 6. Proposed model for the hierarchical organization of Ref(2C)$_4$ films across multiple length scales.

CONCLUSIONS

We have investigated the electrical properties of films from a known reflectin-derived polypeptide originally designed to recapitulate some of the key characteristics of full-length *E. scolopes* reflectins. Within the context of two-terminal devices, these films' conductivities demonstrated distinct kinetic isotope effects, validating the functionality of the reflectin-derived polypeptide as a bulk proton conductor, and possessed high average values of ∼0.4 mS/cm, which were ∼4-fold to ∼8-fold greater than those previously measured for *D. pealeii* reflectin A1 films under analogous conditions. Moreover, the films' conductivity demonstrated a logarithmic dependence on the relative humidity, in agreement with expectations for a proton-conducting material, and maintained a relatively high value across millimeter-scale distances, which were ∼10-fold to ∼20-fold larger than the ones previously reported for device-integrated *D. pealeii* reflectin A1 and A2 films. Taken together, these findings underscored the utility and promise of the reflectin class of proteins as bioelectronic materials.

We have in turn globally characterized our reflectin-derived polypeptide films with a suite of complementary techniques, enabling us to propose a comprehensive model for their hierarchical organization (Figure 6). At the macroscale (i.e., tens of millimeters), the films appear uniform and continuous (Figure 6, far left). At the microscale (i.e., tens of microns), the surfaces of the films are covered by abutting densely packed nanostructures (Figure 6, middle left). At the nanoscale (i.e., tens to hundreds of nanometers), the individual nanostructures appear spheroidal and resemble deformed nanoparticles (Figure 6, middle right). At the molecular scale (i.e., one to several nanometers), the self-assembled polypeptides comprising the nanoparticles exhibit distinct secondary structural order, i.e., primarily α-helical character (Figure 6, far right). The developed nuanced understanding of our films' organization across multiple length scales provides a rationale for our two-terminal devices' electrical characteristics and appears poised to enable more advanced device applications in the future.

We have furthermore studied the local molecular-level structural characteristics of the reflectin-derived polypeptides comprising our films with ssNMR spectroscopy. Such experiments allowed for the identification and assignment of signals corresponding to nearly all of the amino acid types within Ref(2C)$_4$'s four DPRYYDYYGRFNDYDRYYGRSMF repeats (Table S3). Our systematic analysis of the assigned signals revealed that the majority of the repeats' aromatic and aliphatic amino acids, i.e., Tyr, Gly, and Pro, were generally associated with structurally uniform (α-helical) ordered arrangements, whereas the repeats' negatively and positively charged amino acids (i.e., Asp and Arg) were associated with mobile and/or structurally heterogeneous (various α-helical and β-type) arrangements. These findings hint that the reflectin-derived polypeptides' amino acid composition may cause local partitioning of our films into hydrophobic and hydrophilic domains, wherein the conformationally promiscuous charged amino acids facilitate efficient long-range proton transport. Accordingly, our observations and analysis furnish mechanistic insight into the likely molecular-level origins of our reflectin-derived polypeptide films' excellent proton-conducting functionalities.

In summary, our findings hold fundamental and technological significance for several reasons. First, we have explored the electrical properties of a proteinaceous material derived from *E. scolopes* reflectins (rather than from *D. pealeii* reflectins, as previously reported), hinting that the entire reflectin protein class may exhibit proton-conducting functionality. Second, we have demonstrated that our reflectin-derived polypeptide films feature long-range proton conductivities on par with those reported for other proteins and peptides, underscoring reflectins' potential as bioelectronic materials. Third, we have developed a detailed understanding of our films' hierarchical organization and molecular-level ordering, providing reasonable rationales for their performance within two-terminal devices and generally excellent bulk electrical properties. Last, we have added to the current understanding of the relationship between the structure and electrical function of reflectin-based materials, portending favorably for further study of both the reflectin-derived polypeptides' and full-length reflectins' atomic-level structures in the solid state. Given such considerations, our work appears positioned to guide the continued development and engineering of not only reflectins but also other proton-conducting proteins.

ASSOCIATED CONTENT

Supporting Information

The Supporting Information is available free of charge at https://pubs.acs.org/doi/10.1021/acsami.0c18929.

Materials and methods; illustration of the general fabrication scheme, equivalent circuit used for the analysis of the Nyquist plots, comparisons of the experimental and simulated Nyquist plots, dependence of the proton conductivity on the RH, 2D $^{13}C-^{13}C$ correlation ssNMR spectra for different films, and 1D cross section extracted from Figure 5; and tables of key parameters extracted from the Nyquist plots and a table of tabulated characteristics obtained from the assignment and analysis of the ssNMR signals (PDF)

AUTHOR INFORMATION

Corresponding Authors

Bo Chen − *Department of Physics, University of Central Florida, Orlando, Florida 32816, United States;* orcid.org/0000-0001-5589-2075; Email: bo.chen@ucf.edu

https://doi.org/10.1021/acsami.0c18929
ACS Appl. Mater. Interfaces XXXX, XXX, XXX−XXX

Alon A. Gorodetsky − *Department of Materials Science and Engineering, Department of Chemistry, and Department of Chemical and Biomolecular Engineering, University of California, Irvine, Irvine, California 92697, United States;* orcid.org/0000-0002-3811-552X; Email: alon.gorodetsky@uci.edu

Authors

Chengyi Xu − *Department of Materials Science and Engineering, University of California, Irvine, Irvine, California 92697, United States*

Nabin Kandel − *Department of Physics, University of Central Florida, Orlando, Florida 32816, United States*

Xin Qiao − *Department of Physics, University of Central Florida, Orlando, Florida 32816, United States*

Md. Imran Khan − *Department of Physics, University of Central Florida, Orlando, Florida 32816, United States*

Preeta Pratakshya − *Department of Chemistry, University of California, Irvine, Irvine, California 92697, United States*

Nadia E. Tolouei − *Department of Chemical and Biomolecular Engineering, University of California, Irvine, Irvine, California 92697, United States*

Complete contact information is available at: https://pubs.acs.org/10.1021/acsami.0c18929

Author Contributions

N.K., X.Q., and I.K. expressed and purified the protein. C.X. carried out the device fabrication and performed the electrical measurements. C.X. and N.E.T. performed the EIS analysis and equivalent circuit modeling. C.X. performed the optical microscopy, SEM, AFM, and FTIR measurements. C.X. and P.P. performed the DLS, UV/Vis, and CD measurements in solution. P.P. and N.K. performed the ssCD measurements. N.K., X.Q., and I.K. performed the ssNMR measurements. C.X., N.K., P.P., N.T., B.C., and A.A.G. wrote the manuscript.

Funding

The authors are grateful to the Air Force Office of Scientific Research (grants FA2386-14-1-3026 and FA9550-17-1-0024), the Defense Advanced Research Projects Agency (cooperative agreement D16AP00034), the Office of Naval Research (grant N00014-20-1-2265), the UCF P3 Fellowship Program, and the National Science Foundation (grant MCB-1856055). The authors acknowledge the use of facilities and instrumentation at the Irvine Materials Research Institute (IMRI) and at the Laser Spectroscopy Labs (LSL). The authors also acknowledge assistance from Zhehong Gan and Ivan Hung at the National High Magnetic Field Laboratory (grant DMR-1157490) and the State of Florida as well as from the Mass Spectrometry Research and Education Center (grant NIH S10 OD021758-01A1).

Notes

The authors declare no competing financial interest.

The authors thank Patrick Dennis from the Air Force Research Laboratory for kind donation of the plasmid necessary for expression of the polypeptide.

All data needed to evaluate the conclusions in the paper are present in the main text and/or the Supporting Information.

REFERENCES

(1) Irimia-Vladu, M., Glowacki, E. D., Sariciftci, N. S., Bauer, S. *Green Materials for Electronics*, 1st ed., Wiley−VCH, 2017.

(2) Selyanchyn, O.; Selyanchyn, R.; Lyth, S. M. A Review of Proton Conductivity in Cellulosic Materials. *Front. Energy Res.* **2020**, *8*, 596164.

(3) Vahidzadeh, E.; Kalra, A. P.; Shankar, K. Melanin-Based Electronics: From Proton Conductors to Photovoltaics and Beyond. *Biosens. Bioelectron.* **2018**, *122*, 127−139.

(4) Strakosas, X.; Selberg, J.; Hemmatian, Z.; Rolandi, M. Taking Electrons out of Bioelectronics: From Bioprotonic Transistors to Ion Channels. *Adv. Sci.* **2017**, *4*, 1600527.

(5) Meredith, P.; Bettinger, C. J.; Irimia-Vladu, M.; Mostert, A. B.; Schwenn, P. E. Electronic and Optoelectronic Materials and Devices Inspired by Nature. *Rep. Prog. Phys.* **2013**, *76*, 34501.

(6) Amdursky, N.; Głowacki, E. D.; Meredith, P. Macroscale Biomolecular Electronics and Ionics. *Adv. Mater.* **2019**, *31*, 1802221.

(7) Miyake, T.; Rolandi, M. Grotthuss Mechanisms: From Proton Transport in Proton Wires to Bioprotonic Devices. *J. Phys. Condens. Matter* **2016**, *28*, No. 023001.

(8) Torculas, M.; Medina, J.; Xue, W.; Hu, X. Protein-Based Bioelectronics. *ACS Biomater. Sci. Eng.* **2016**, *2*, 1211−1223.

(9) Carter, N. A.; Grove, T. Z. Functional Protein Materials: Beyond Elastomeric and Structural Proteins. *Polym. Chem.* **2019**, *10*, 2952−2959.

(10) Kautz, R.; Ordinario, D. D.; Tyagi, V.; Patel, P.; Nguyen, T. N.; Gorodetsky, A. A. Cephalopod-Derived Biopolymers for Ionic and Protonic Transistors. *Adv. Mater.* **2018**, *30*, 1704917.

(11) Silberbush, O.; Engel, M.; Sivron, I.; Roy, S.; Ashkenasy, N. Self-Assembled Peptide Nanotube Films with High Proton Conductivity. *J. Phys. Chem. B* **2019**, *123*, 9882−9888.

(12) Mondal, S.; Agam, Y.; Nandi, R.; Amdursky, N. Exploring Long-Range Proton Conduction, the Conduction Mechanism and Inner Hydration State of Protein Biopolymers. *Chem. Sci.* **2020**, *11*, 3547−3556.

(13) Carter, N. A.; Grove, T. Z. Protein Self-Assemblies That Can Generate, Hold, and Discharge Electric Potential in Response to Changes in Relative Humidity. *J. Am. Chem. Soc.* **2018**, *140*, 7144−7151.

(14) Silberbush, O.; Amit, M.; Roy, S.; Ashkenasy, N. Significant Enhancement of Proton Transport in Bioinspired Peptide Fibrils by Single Acidic or Basic Amino Acid Mutation. *Adv. Funct. Mater.* **2017**, *27*, 1604624.

(15) Amdursky, N.; Wang, X.; Meredith, P.; Bradley, D. D. C.; Stevens, M. M. Long-Range Proton Conduction across Free-Standing Serum Albumin Mats. *Adv. Mater.* **2016**, *28*, 2692−2698.

(16) Pena-Francesch, A.; Jung, H.; Hickner, M. A.; Tyagi, M.; Allen, B. D.; Demirel, M. C. Programmable Proton Conduction in Stretchable and Self-Healing Proteins. *Chem. Mater.* **2018**, *30*, 898−905.

(17) Chatterjee, A.; Norton-Baker, B.; Bagge, L. E.; Patel, P.; Gorodetsky, A. A. An Introduction to Color-Changing Systems from the Cephalopod Protein Reflectin. *Bioinspir. Biomim.* **2018**, *13*, No. 045001.

(18) Ordinario, D. D.; Phan, L.; Walkup, W. G., IV; Jocson, J.-M.; Karshalev, E.; Hüsken, N.; Gorodetsky, A. A. Bulk Protonic Conductivity in a Cephalopod Structural Protein. *Nat. Chem.* **2014**, *6*, 596−602.

(19) Ordinario, D. D.; Phan, L.; Walkup, W. G., IV; Van Dyke, Y.; Leung, E. M.; Nguyen, M.; Smith, A. G.; Kerr, J.; Naeim, M.; Kymissis, I.; Gorodetsky, A. A. Production and Electrical Characterization of the Reflectin A2 Isoform from Doryteuthis (Loligo) Pealeii. *RSC Adv.* **2016**, *6*, 57103−57107.

(20) Ordinario, D. D.; Phan, L.; Jocson, J.-M.; Nguyen, T.; Gorodetsky, A. A. Protonic Transistors from Thin Reflectin Films. *APL Mater.* **2015**, *3*, No. 014907.

(21) Ordinario, D. D.; Phan, L.; Van Dyke, Y.; Nguyen, T.; Smith, A. G.; Nguyen, M.; Mofid, N. M.; Dao, M. K.; Gorodetsky, A. A. Photochemical Doping of Protonic Transistors from a Cephalopod Protein. *Chem. Mater.* **2016**, *28*, 3703−3710.

(22) Ordinario, D. D.; Leung, E. M.; Phan, L.; Kautz, R.; Lee, W. K.; Naeim, M.; Kerr, J. P.; Aquino, M. J.; Sheehan, P. E.; Gorodetsky, A.

A. Protochromic Devices from a Cephalopod Structural Protein. *Adv. Opt. Mater.* **2017**, *5*, 1600751.
(23) Lu, Y.; Pratakshya, P.; Chatterjee, A.; Jia, X.; Ordinario, D. D.; Phan, L.; Sanchez, J. A. C.; Kautz, R.; Tyagi, V.; Patel, P.; Dyke, Y. V.; Dao, M. K.; Couvrette, J.; Kerr, J. P.; Long, J.; Allevato, A.; Leal-Cruz, J.; Tseng, E.; Peng, E. R.; Reuter, A.; Drake, S.; Omenetto, F.; Gorodetsky, A. A. Aqueous Processing of the Conductive Cephalopod Protein Reflectin via Inkjet Printing. *APL Mater.* **2020**, *8*, 101113.
(24) Crookes, W. J.; Ding, L.-L.; Huang, Q. L.; Kimbell, J. R.; Horwitz, J.; McFall-Ngai, M. J. Reflectins: The Unusual Proteins of Squid Reflective Tissues. *Science* **2004**, *303*, 235−238.
(25) Kramer, R. M.; Crookes-Goodson, W. J.; Naik, R. R. The Self-Organizing Properties of Squid Reflectin Protein. *Nat. Mater.* **2007**, *6*, 533−538.
(26) Qin, G.; Dennis, P. B.; Zhang, Y.; Hu, X.; Bressner, J. E.; Sun, Z.; Crookes-Goodson, W. J.; Naik, R. R.; Omenetto, F. G.; Kaplan, D. L. Recombinant Reflectin-Based Optical Materials. *J. Polym. Sci., Part B: Polym. Phys.* **2013**, *51*, 254−264.
(27) Dennis, P. B.; Singh, K. M.; Vasudev, M. C.; Naik, R. R.; Crookes-Goodson, W. J. Research Update: A Minimal Region of Squid Reflectin for Vapor-Induced Light Scattering. *APL Mater.* **2017**, *5*, 120701.
(28) Phan, L.; Walkup, W. G., IV; Ordinario, D. D.; Karshalev, E.; Jocson, J.-M.; Burke, A. M.; Gorodetsky, A. A. Reconfigurable Infrared Camouflage Coatings from a Cephalopod Protein. *Adv. Mater.* **2013**, *25*, 5621−5625.
(29) Phan, L.; Ordinario, D. D.; Karshalev, E.; Walkup, W. G., IV; Shenk, M. A.; Gorodetsky, A. A. Infrared Invisibility Stickers Inspired by Cephalopods. *J. Mater. Chem. C* **2015**, *3*, 6493−6498.
(30) Naughton, K. L.; Phan, L.; Leung, E. M.; Kautz, R.; Lin, Q.; Van Dyke, Y.; Marmiroli, B.; Sartori, B.; Arvai, A.; Li, S.; Pique, M. E.; Naeim, M.; Kerr, J. P.; Aquino, M. J.; Roberts, V. A.; Getzoff, E. D.; Zhu, C.; Bernstorff, S.; Gorodetsky, A. A. Self-Assembly of the Cephalopod Protein Reflectin. *Adv. Mater.* **2016**, *28*, 8405−8412.
(31) Colomer, I.; Chamberlain, A. E. R.; Haughey, M. B.; Donohoe, T. J. Hexafluoroisopropanol as a Highly Versatile Solvent. *Nat. Rev. Chem.* **2017**, *1*, 0088.
(32) Hirota, N.; Goto, Y.; Mizuno, K. Cooperative α-Helix Formation of β-Lactoglobulin and Melittin Induced by Hexafluoroisopropanol. *Protein Sci.* **1997**, *6*, 416−421.
(33) Bohren, C. F.; Huffman, D. R. *Absorption and Scattering of Light by Small Particles*; Wiley−VCH, 1998, DOI: 10.1002/9783527618156.
(34) Chatterjee, A.; Sanchez, J. A. C.; Yamauchi, T.; Taupin, V.; Couvrette, J.; Gorodetsky, A. A. Cephalopod-Inspired Optical Engineering of Human Cells. *Nat. Commun.* **2020**, *11*, 2708.
(35) Chemes, L. B.; Alonso, L. G.; Noval, M. G.; de Prat-Gay, G. Circular Dichroism Techniques for the Analysis of Intrinsically Disordered Proteins and Domains. *Methods Mol. Biol.* **2012**, *895*, 387−404.
(36) Kelly, S. M.; Jess, T. J.; Price, N. C. How to Study Proteins by Circular Dichroism. *Biochim. Biophys. Acta* **2005**, *1751*, 119−139.
(37) Mei, B.-A.; Munteshari, O.; Lau, J.; Dunn, B.; Pilon, L. Physical Interpretations of Nyquist Plots for EDLC Electrodes and Devices. *J. Phys. Chem. C* **2018**, *122*, 194−206.
(38) Soboleva, T.; Xie, Z.; Shi, Z.; Tsang, E.; Navessin, T.; Holdcroft, S. Investigation of the Through-Plane Impedance Technique for Evaluation of Anisotropy of Proton Conducting Polymer Membranes. *J. Electroanal. Chem.* **2008**, *622*, 145−152.
(39) Agmon, N. The Grotthuss Mechanism. *Chem. Phys. Lett.* **1995**, *244*, 456−462.
(40) Springer, T. E.; Zawodzinski, T. A.; Gottesfeld, S. Polymer Electrolyte Fuel Cell Model. *J. Electrochem. Soc.* **1991**, *138*, 2334.
(41) Zawodzinski, T. A.; Davey, J.; Valerio, J.; Gottesfeld, S. The Water Content Dependence of Electro-Osmotic Drag in Proton-Conducting Polymer Electrolytes. *Electrochim. Acta* **1995**, *40*, 297−302.
(42) Barth, A. Infrared Spectroscopy of Proteins. *Biochim. Biophys. Acta - Bioenerg.* **2007**, *1767*, 1073−1101.
(43) Berthomieu, C.; Hienerwadel, R. Fourier Transform Infrared (FTIR) Spectroscopy. *Photosynth. Res.* **2009**, *101*, 157−170.
(44) Jeon, J.; Qiao, X.; Hung, I.; Mitra, A. K.; Desfosses, A.; Huang, D.; Gor'kov, P. L.; Craven, R. C.; Kingston, R. L.; Gan, Z.; Zhu, F.; Chen, B. Structural Model of the Tubular Assembly of the Rous Sarcoma Virus Capsid Protein. *J. Am. Chem. Soc.* **2017**, *139*, 2006−2013.
(45) Wishart, D. S.; Bigam, C. G.; Holm, A.; Hodges, R. S.; Sykes, B. D. ^{1}H, ^{13}C and ^{15}N Random Coil NMR Chemical Shifts of the Common Amino Acids. I. Investigations of Nearest-Neighbor Effects. *J. Biomol. NMR* **1995**, *5*, 67−81.
(46) Kolodziejski, W.; Klinowski, J. Kinetics of Cross-Polarization in Solid-State NMR: A Guide for Chemists. *Chem. Rev.* **2002**, *102*, 613−628.
(47) Hu, K.-N.; Tycko, R. What can Solid State NMR Contribute to Our Understanding of Protein Folding? *Biophys. Chem.* **2010**, *151*, 10−21.
(48) Tycko, R. Solid-State NMR Studies of Amyloid Fibril Structure. *Ann. Rev. Phys. Chem.* **2011**, *62*, 279−299.
(49) Su, Y.; Hong, M. Conformational Disorder of Membrane Peptides Investigated from Solid-State NMR Line Widths and Line Shapes. *J. Phys. Chem. B* **2011**, *115*, 10758−10767.
(50) Quinn, C. M.; Wang, M.; Fritz, M. P.; Runge, B.; Ahn, J.; Xu, C.; Perilla, J. R.; Gronenborn, A. M.; Polenova, T. Dynamic Regulation of HIV-1 Capsid Interaction with the Restriction Factor TRIM5α Identified by Magic-Angle Spinning NMR and Molecular Dynamics Simulations. *Proc. Natl. Acad. Sci. U.S.A.* **2018**, *115*, 11519−11524.

https://doi.org/10.1021/acsami.0c18929
ACS Appl. Mater. Interfaces XXXX, XXX, XXX−XXX